RSC Advances

Core/shell-structured nickel ferrite/onion-like carbon nanocapsules: An anode material with enhanced electrochemical performance for lithium-ion batteries

SCHOLARONE™
Manuscripts

RSC Advances

Dynamic Article Links ▶

PAPER

Core/shell-structured nickel ferrite/onion-like carbon nanocapsules: An anode material with enhanced electrochemical performance for lithium-ion batteries

Dandan Han,[*a] **Gengxin Song,**[a] **Bao Liu,**[a] **and He Yan**[a]

Core/shell-structured nanocapsules consisting of a nickel ferrite ($NiFe_2O_4$) nanoparticle core encapsulated in an onion-like carbon (C) shell are prepared by a modified arc-discharge method followed by an air-annealing process. Lithium-ion batteries fabricated using the nanocapsules as the anode material
10 exhibit the stable specific capacity of 914 mAh g^{-1} after 500 cycles at a current density of 0.1 C. Varying the rate of charge/discharge current from 0.1 to 4 C does not show negative effects on the recycling stability of the nanocapsules and a recoverable specific capacity as high as 914 mAh g^{-1} is obtained. The introduction of the onion-like C shell and the presence of the void spaces are found to increase the contact areas between the electrolyte and the nanocapsules for improved electrolyte diffusion, to enhance the
15 electronic conductivity and ionic mobility of the $NiFe_2O_4$ nanoparticle cores, and to accommodate the change in volume during the lithium-ion insertion/extraction process.

1. Introduction

Recently, increasing research efforts have been triggered in developing high-performance electrode materials for advanced
20 lithium-ion batteries（LIBs）to meet the ever-growing demands for electrochemical energy storage.[1] To apply LIBs in electric vehicles and renewable energy storage, a significant advance in energy storage density, power density, and cycle life is required.[2] The current commercial anode material for LIBs, graphite, is
25 limited to a low theoretical capacity of 372 mAh g^{-1}. Meanwhile, the possible reaction between lithiated graphite and the electrolyte is an inherent safety risk.[3] Therefore, much effort has been devoted to develop anode materials with high capacity, long cycling stability, and high rate capability.[4]
30 Transition metal oxides (TMO) nanostructures have attracted broad attention because of their advantages of high surface-to-volume ratio and short path length for Li-ion diffusion in comparison with their bulk counterparts. Various kinds of TMO nanostructures, such as Co_3O_4, CuO, SnO_2, NiO, Fe_2O_3, Fe_3O_4,
35 have been widely investigated as the alternative anode materials for use in LIBs over the past decade because of their high specific capacity (500 to 1000 mAh g^{-1}).[5-11] Recently, some ternary transition metal oxides (AB_2O_4, A, B=transition metal), which also crystallizes in a spinel structure, can react reversibly with
40 lithium ions according to the following reversible reaction: $AB_2O_4+8e^-+8Li^+\leftrightarrow A+2B+4Li_2O$.[12] Thus, they can provide twice the capacity per unit mass and three times the density, which is very suitable for anodes of LIBs. Among AB_2O_4, $NiFe_2O_4$ has an inverse spinel structure in which, in its ideal state, all Ni^{2+} ions
45 are in B sites and Fe^{3+} ions are equally distributed between A and B sites.[13] $NiFe_2O_4$ has been widely studied due to its low toxicity,

low cost, high thermal stability and especially its excellent electrochemical performance with high initial discharge capacity.[14] As the performance of $NiFe_2O_4$ is highly dependent on
50 the micro-/nanostructures of the materials in various applications, so far a series of $NiFe_2O_4$ nanostructures has been reported. Macroporous $NiFe_2O_4$ was synthesized through a sol-gel method which delivered a capacity of 600 mAh g^{-1} after 80 cycles at the rate of 1C, but it was lack of long term cycling performance.[15]
55 $NiFe_2O_4$ nanocrystalline was prepared by anodization of the alloy films at room temperature and exhibited a low reversible capacity of 355 mAh g^{-1}.[16] $NiFe_2O_4$ nanorods were synthesized by a template-engaged reaction, with β-FeOOH nanorods as precursors which were prepared by a hydrothermal method and
60 retained the reversible capacity of 520 mAh g^{-1} at the current density of 1 A g^{-1} after 300 cycles.[3] However, the cycling stability is still not very satisfactory for practical applications due to the drastic volume change during the charge-discharge process. The volume change can cause the pulverization of the electrode and
65 breaks down the electrical contact pathways between adjacent particles, thus leading to rapid capacity fading and poor cycling stability, which impose restrictions on its commercial implementations.[17] In this regard, the commonly used approach is to make nanocomposite materials, particularly with carbon,
70 where the function of carbon is twofold: providing a physical buffering layer for the large volume change (cushion effect) and increasing the electrical conductivity.[9] Among the numerous carbon materials, onion-like carbon layers has been widely investigated for its unique characteristics, such as chemical
75 stability, high electrical conductivity, and large surface area. These encouraging characteristics provide such onion-like carbon layers with a wide range of potential applications and have

attracted great interest in the development of composites with other materials.[18]

The core/shell-type nanocomposite, named by nanocapsules, is widely used as anode materials for LIBs, due to the improved cycling behavior and enhanced kinetics of lithium intercalation and de-intercalation.[19] Liu et al have successfully prepared onion-like C-coated CuO, Co_3O_4, NiO and Sn nanocapsules and have demonstrated the enhanced electrochemical performances.[6,7,9,20] The onion-like C shell provides a void space for the volume changes and improves the electron conductivity.[6-9] Therefore, the development of core/shell-structured nanocapsules with $NiFe_2O_4$ nanoparticles as the core and onion-like C as the shell is imperative to new generation anode materials in high-performance LIBs. In the present work, core/shell-structured $NiFe_2O_4$/onion-like C nanocapsules have been prepared by a modified arc-discharge method followed by an air-annealing process. For comparison, the $NiFe_2O_4$ nanoparticles without onion-like carbon layers also are synthesized at the same condition. The electrochemical performances of $NiFe_2O_4$/onion-like C nanocapsules as an anode for LIBs are investigated in detail, in particular concerning the influence of the onion-like carbon layer shell on the discharge capacity, initial coulomb efficiency, cycle performance and rate capability of $NiFe_2O_4$ nanoparticles.

2. Experimental

2.1 Materials

Nickel (Ni) powder, iron (Fe) powder and absolute ethyl alcohol (C_2H_5OH) are obtained from Shanghai Chemical Company (Shanghai, China). All chemicals are of analytical grade and used without further purification.

2.2 Synthesis of $NiFe_2O_4$/onion-like C nanocapsules

Spherical FeNi/C nanocapsules consisting of FeNi cores and onion-like C shells were prepared by a modified arc discharge method.[21, 22] A master nominal composition $NiFe_2$ alloy was prepared by arc melting Fe and Ni bulk pieces of 99.9 wt% purity under high-purity argon atmosphere. In the arc-discharge process, a $NiFe_2$ alloy served as the anode, while the cathode was a carbon needle. The anode target was placed into one pit of a water-cooled carbon crucible. After the chamber was evacuated in a vacuum of 6.0×10^{-3} Pa, liquid ethanol of 20 ml was introduced into the chamber together with a mixture of Ar (16000 Pa) and H_2 (5000 Pa) as a reactant gas and a source of hydrogen plasma. During the experimental process, the current was maintained at 80 A for 0.5 h. After being passivated in 0.01 MPa air for 24h, the products were collected from depositions on the top of the water-cooled chamber. To prepare the $NiFe_2O_4$/onion-like C nanocapsules and $NiFe_2O_4$ nanoparticles, the FeNi/onion-like C nanocapsules were put on an Al_2O_3 crucible and were annealed at 150 and 300 ^{o}C for 1 h in a tubular furnace in still air, respectively.

2.3 Materials characterizations

Phase, morphology and microstructure of the as-prepared samples were characterized by X-ray diffraction (XRD, Bruker D8 Advance) and transmission electron microscopy (TEM, JEM-2010) with an emission voltage of 200 kV. X-ray photoelectron spectroscopy (XPS) measurement were performed on an ESCALAB-250 with a monochromatic X-ray source (an aluminum K_α line of 1486.6 eV energy and 150 W). The electrochemical tests were performed under ambient temperature using standard R2032 type coin cells with lithium serving as both the counter electrode and the reference electrode. The working electrodes were prepared by mixing the $NiFe_2O_4$/onion-like C nanocapsules, conductivity agent (acetylene black), and poly(vinyl difluoride) at a weight ratio of 50:30:20 and by pasting with pure Cu foil. 1 M $LiPF_6$ in ethylene carbonate-diethyl carbonate (1:1 in volume) was employed as the electrolyte. The cells were assembled in an argon-filled glove box with both the moisture and the oxygen content below 1 ppm. Galvanostatic charge-discharge was carried out using a land battery program-control test system (Wuhan, China) in the potential range of 0.01-3.0 V at a setting current rate. The cyclic voltammetry (CV) test was implemented using an electrochemical workstation (Model 2273, Princeton Applied Research, USA). Electrochemical impedance spectroscopy (EIS) measurements were performed on this apparatus over a frequency range of 0.01 Hz- 0.1 MHz at different charge-discharge stages.
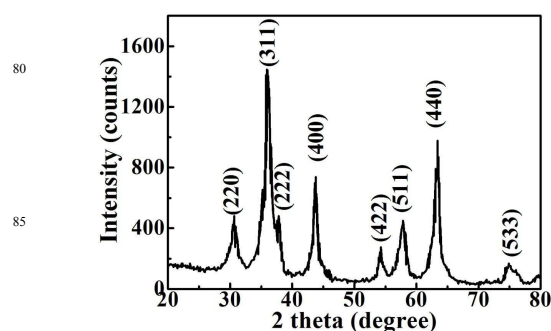
3. Results and Discussion

Fig.1. XRD pattern of the $NiFe_2O_4$/onion-like C nanocapsules.

Fig. 1 shows the typical XRD pattern of the as-prepared $NiFe_2O_4$/onion-like C nanocapsules. As evident, the diffraction peaks at 2θ values of 30.6^o, 36.0^o, 37.8^o, 43.8^o, 54.3^o, 57.8^o, 63.4^o and 74.9^o are indexed to the reflection of (220), (311), (222), (400), (422), (511), (440) and (533) planes comparing with the standard pattern (JCPDS No.10-0325). In addition, it should be noted that there are no peaks of pure C, suggesting its small amount (less than 3% in the products), if any.[6-9,21] Carbon atoms are usually favorable to form the shell of nanoparticles in an onion-like structure, which is difficult to detect because of breaking down of the periodic boundary condition (translation symmetry) along the radial direction.[6-9]

Fig.2 presents the representative TEM images of $NiFe_2O_4$/C nanocapsules. TEM image in Fig.2(a) shows spherical samples with a diameter in the range of 5 to 60 nm. The averaged particle size obtained by measuring more than 200 particles is estimated to be 31.3 nm. The HRTEM image in Fig.2(b) clearly indicates that the nanoparticles own a clear 'core/shell' type structure, in which the inner nanoparticles cores are encapsulated by the onion-like cages. The lattice plane spacing of the onion-like cages is about 0.34 nm, corresponding to the (002) plane of graphite. Nevertheless, a mass of lattice imperfections can be

seen in the carbon layers as a consequence of the serious bending and collapsing of the graphite atom layer, which is similar with NiO/C, CuO/C and Co_3O_4/C nanocapsules.[6, 7, 9] The measured interplanar of 0.2 nm in the nanoparticles can be assigned to the characteristic interplanar distance of (400) of $NiFe_2O_4$. It is clearly noted that there is a hollow structure between $NiFe_2O_4$ nanoparticles and onion-like C shells, which can provide enough void spaces to accommodate the volume change of the $NiFe_2O_4$ nanoparticles during the charge/discharge process and can help the nanoparticles during cycling keep the state of aggregation.
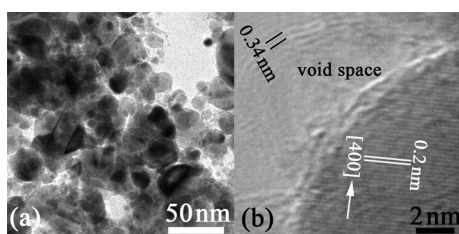

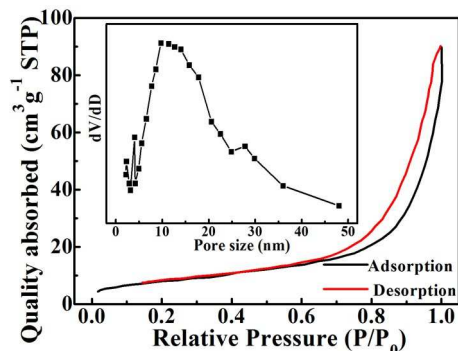Fig.2. (a) TEM and (b) HRTEM images of $NiFe_2O_4$/onion-like C nanocapsules.

Fig.3. N_2 adsorption-desorption isotherm and PSD data (the inset) of the $NiFe_2O_4$/onion-like C nanocapsules.
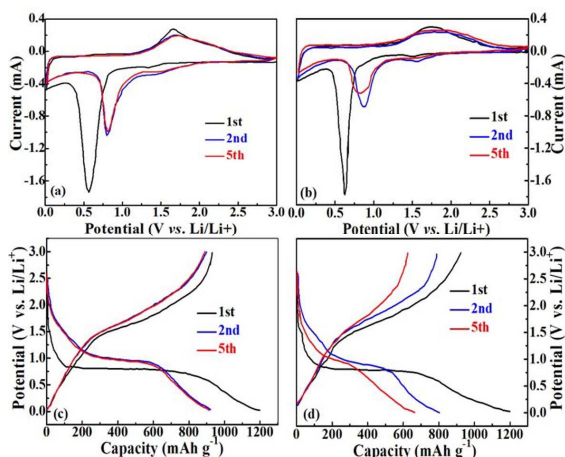

Fig.4. CV curves and the corresponding charge/discharge voltage profiles of (a,c) $NiFe_2O_4$/onion-like C nanocapsules and (b,d) $NiFe_2O_4$ nanoparticles for the selected cycles in voltage range of 0.01- 3.0 V at a scan rate of 0.1 mV s^{-1}.

The N_2 adsorption-desorption measurement at a liquid N_2 temperature of 77 K is further performed to study the void space of $NiFe_2O_4$/onion-like C nanocapsules. Fig.3 depicts the adsorption-desorption isotherm and pore size distribution (PSD) for $NiFe_2O_4$/onion-like C nanocapsules. Obviously, a distinct hysteresis loop with the typical IV sorption behavior shown in Fig.3 indicates the typical mesoporous feature. Additionally, as shown in the inset of Fig.3, the $NiFe_2O_4$/onion-like C nanocapsules possess a narrow PSD with a sharp peak at~ 10 nm, resulting from the controlled gas release during the calcinating process. The Brunauer-Emmett-Teller (BET) void space volume and the average void space size are 0.132 cm^3 g^{-1} and 14 nm, respectively.
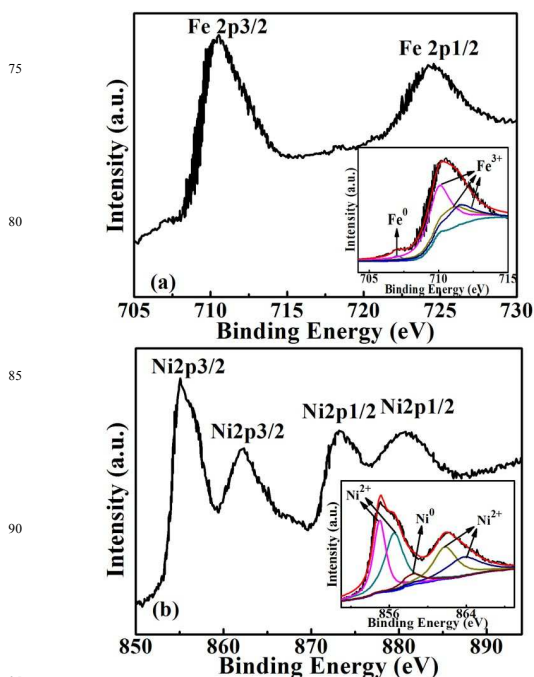

Fig.5. XPS spectra of (a) Fe 2p and (b) Ni 2p for the $NiFe_2O_4$/onion-like C nanocapsules. Both spectra are obtained after the first charge up to 3.0 V. Inset: the fitting curves.

Coin-type cell configuration has been used to evaluate the applicability of the $NiFe_2O_4$/onion-like C nanocapsules as an anode material for high-performance LIBs, and the results are compared with the $NiFe_2O_4$ nanoparticles electrode. The electrochemical activity with respect to Li insertion/extraction is first evaluated by CV. Figs.4(a) and 4(b) depict the CV curves of the $NiFe_2O_4$/onion-like C nanocapsules and the $NiFe_2O_4$ nanoparticles for the selected cycles in the voltage range of 0.01-3.0 V at a scan rate of 0.1 mV s^{-1}. In the first scan, two cathodic peaks are observed at 0.56 and 1.33 V for $NiFe_2O_4$/onion-like C nanocapsules and 0.63 and 1.50 V for $NiFe_2O_4$ nanoparticles, corresponding to the conversion reactions of Fe^{3+} and Ni^{2+} to metallic Fe and Ni, the formation of Li_2O and the irreversible reaction with electrolyte to form a solid electrolyte interphase (SEI) film.[23] In the subsequent cycles, the cathodic peaks tend to positively shift, which may be related to a structure rearrangement and associated with the reversible reduction of

Fe^{3+} and Ni^{2+}.[3] The broad anodic peaks around 1.56 - 1.90 V can be ascribed to the oxidation of Fe to Fe^{3+} and Co to Co^{2+}. As shown in Fig.4 (b), the intensity of the peaks changes with cycle numbers, which indicates poor cycling stability of the $NiFe_2O_4$ nanoparticles. Note that the CV curves remain unchanged after the first cycle, suggesting the excellent cycling stability of the $NiFe_2O_4$/onion-like C nanocapsules. In order to investigate the mechanisms of $NiFe_2O_4$/onion-like C nanocapsules during the charge-discharge process, the XPS spectra of Fe 2p and Ni 2p are shown in Fig.5, which are obtained after the first charge up to 3.0 V. The fitting peaks of Fe and Ni are shown in the inset of Fig.5(a) and (b), respectively, which are based on the Gaussian-Lorentzian mixed function. The peaks at 709.9 eV, 711 eV and 711.5 eV are indentified to Fe^{3+}, while the peak at 707 eV is from the Fe^0.[24-27] As shown in the inset of Fig.5(b), the peaks at 855.02 eV, 856.5 eV, 861.5 eV and 864.1 eV correspond to Ni^{2+}, while the peak at 858.6 eV correspond to Ni^0.[28-30] Based on the CV results, XPS data and the storage mechanisms of $NiFe_2O_4$, the whole electrochemical reactions during the charge-discharge process are believed to be as follows:[3, 14,31-33]
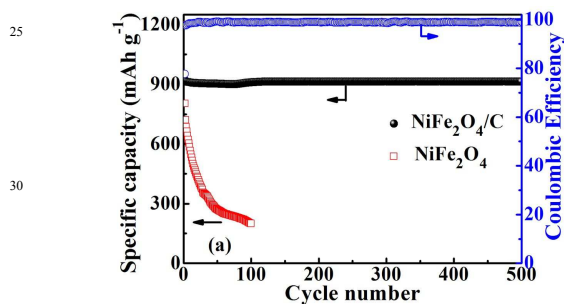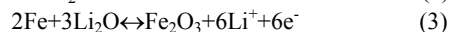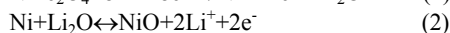
$$NiFe_2O_4 + 8Li^+ + 8e^- \rightarrow Ni + 2Fe + 4Li_2O \quad (1)$$
$$Ni + Li_2O \leftrightarrow NiO + 2Li^+ + 2e^- \quad (2)$$
$$2Fe + 3Li_2O \leftrightarrow Fe_2O_3 + 6Li^+ + 6e^- \quad (3)$$

Fig. 6. The cycling performance and Coulombic efficiency of $NiFe_2O_4$/onion-like C nanocapsules and $NiFe_2O_4$ nanoparticles electrode at a current density of 0.1 C.

Figs. 4(c) and 4(d) show the galvanostatic charge/discharge cycling of $NiFe_2O_4$/onion-like C nanocapsules and $NiFe_2O_4$ nanoparticles at a current density of 0.1 C (91.5 mA g^{-1}) with a voltage range of 0.01-3.0 V. It can be seen that both of the samples show a sudden drop from 3.0 to 1.6 V in discharge profiles, which could be ascribed to few lithium-intercalation occur above 1.6 V.[34] Consistent with the above CV analysis, similar current peaks can be indentified in the voltage profiles of $NiFe_2O_4$/onion-like C nanocapsules and $NiFe_2O_4$ nanoparticles. Both of the electrodes mainly include two regions in the first discharge process, a long flat voltage plateau near 0. 80 V associated with a slope to 0.01 V. For the following cycles, the discharge potential plateau shifts upward to near 1.0 V followed by a more sloping profile, due to different electrochemical reactions as in Eqs. (2) and (3). The initial discharge and charge capacities are 1198.2 and 930.8 mAh g^{-1} for $NiFe_2O_4$/onion-like C nanocapsules, 1198.8 and 923.7 mAh g^{-1} for $NiFe_2O_4$ nanoparticles, corresponding to the coulombic efficiency of 77.7% and 77.1%, respectively. The large irreversible capacity loss in the first cycle could be attributed to the formation of SEI

layer, some undecomposed Li_2O phase and the irreversible decomposition of electrolyte.[27] After first cycles, the discharge capacity of the $NiFe_2O_4$/onion-like C nanocapsules decays more slowly than that of the $NiFe_2O_4$ nanoparticles, as shown in Figs.4(c) and 4(d). The above results indicate that the $NiFe_2O_4$ nanoparticles show a higher initial capacity but with worse retention.

To further reveal the excellent properties of the $NiFe_2O_4$/onion-like C nanocapsules as anode for high-power LIBs, the long-term cycling behavior at 0.1 C and rate capability are further considered in greater detail. Fig.6 depicts discharge specific capacity and Coulombic efficiency with cycling at a current density of 0.1 C. For comparison, the cycling performance of $NiFe_2O_4$ nanoparticles is also presented. There were large initial capacity losses for both electrodes, which are considered inevitable due to the formation of a solid electrolyte interface (SEI) on the electrode surface.[34] After the initial large drop, the capacity of the $NiFe_2O_4$/onion-like C electrode continued to slightly decrease with increasing cycles for the first 75 cycles. Hereafter, the capacity begins to increase and achieves 914 mAh g^{-1} after 500 cycles. The capacity recovery phenomenon after a few initial cycles could from a polymeric gel-like film formation from kinetically activated electrolyte degradation.[1, 35-40] The interesting phenomenon is normally observed for the transition metal oxides in the well-documented literature.[36-39] The excellent performance is the same as the theoretical capacity of 915 mAh g^{-1}, and a rough comparison indicates that the reversible capacity is better than those previously reported.[13-15,17,18] The theoretical capacity of 915 mAh g^{-1} is predicted by the conversion reaction mechanism and calculated by the number of transferred electronics in the reaction.[41] However, this is just an estimated result. Actually, the phenomenon has been reported several times, yet the measured capacity was higher than or near to the theoretical capacity.[42-44] Since battery capacity depends on all the materials available to react, the defective onion-like C with large surface area would display higher reversible capacities that exceeded theoretical capacity because Li^+ ions stored in the defects of the onion-like C shells could take part in the reaction. From the second cycle onward, the coulombic efficiency exhibits a rapid increase and it keeps stable around 99% in the following 15-500 cycles, manifesting that the perfectly crystalline $NiFe_2O_4$ nanoparticles coated by onion-like C shells form a stable structure on the microscale and that the electrochemical Li^+ insertion/extraction process is completely reversible.[17,45] By contrast, the discharge capacity of the $NiFe_2O_4$ nanoparticles drops to 200 mAh g^{-1} after 100 cycles. The poor cycle life of the $NiFe_2O_4$ nanoparticles is mainly due to the larger volume change and the electronic accumulation of the $NiFe_2O_4$ nanoparticles.[46]

A high rate capability is an important parameter for materials in LIBs, mainly because it reduces the discharge-charge time in practical applications.[47] The rate performance of $NiFe_2O_4$/onion-like C at various charge-discharge current densities are investigated and shown in Fig.7. The $NiFe_2O_4$/onion-like C nanocapsules electrode was cycled at different current densities ranging from 0.1 to 4 C. The cell shows good rate capability with average discharge capacity of 910, 874, 832, 760 and 665mAh g^{-1}, when the current density increased stepwise to 0.1, 0.2, 0.5, 2, and 4 C, respectively. Upon altering

the current density back to 0.1 C, the $NiFe_2O_4$/C nanocapsules still deliver an average discharge capacity of 914 mAh g^{-1}, almost no capacity loss after 120 cycles. The result suggests that $NiFe_2O_4$/onion-like C nanocapsules favors high-rate

5 charge/discharge application. By virtue of its core/shell-type structure, the $NiFe_2O_4$/onion-like C nanocapsules show an excellent cycling response to the continuously varied current density.[48] To confirm the stability of the $NiFe_2O_4$ nanoparticles in the $NiFe_2O_4$/onion-like C nanocapsules electrode, the changes in

10 their morphology are examined after 500 cycles under TEM observation, is shown in the inset of Fig. 7. The $NiFe_2O_4$ nanoparticles maintained sphere-like shape, confirming the intact protection offered by the onion-like C shell.
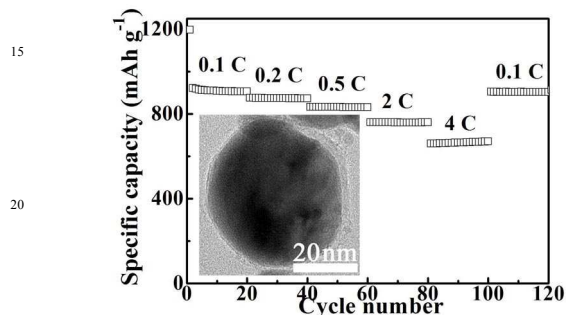

15

20

25 Fig.7. Rate capability of the $NiFe_2O_4$/onion-like C nanocapsules anode. The inset shows the TEM image of $NiFe_2O_4$/onion-like C nanocapsules electrodes after 500 cycles.

Furthermore, in order to reveal the transport kinetics for the

30 electrochemical properties of $NiFe_2O_4$/onion-like C nanocapsules, EIS measurements were carried out after 50 cycles at the current density of 0.1 C. As shown in Fig.8, the impedance spectra consisted of one compressed semicircles in the middle frequency region, which was related to the charge transfer resistance R_{ct}, and

35 a line in the low-frequency range, which could be considered as Warburg impedance (Z_w). The charge transfer resistances of $NiFe_2O_4$/onion-like C nanocapsules is 52 Ω, which is lower than that (75 Ω) of $NiFe_2O_4$ nanoparticle. It may state that the onion-like carbon shell in $NiFe_2O_4$/onion-like C nanocapsules may

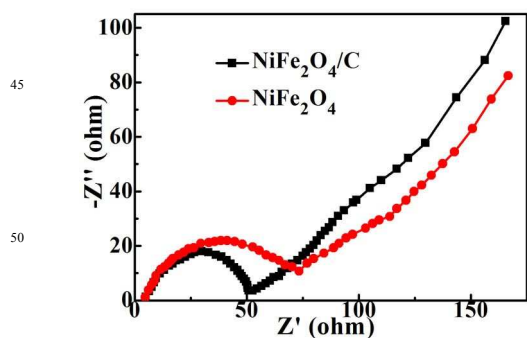40 favor the electronic transmission and lead to a small internal resistance as well as good capacity retention.[49]

45

50

Fig.8. EIS spectra of $NiFe_2O_4$/onion-like C nanocapsules and

55 $NiFe_2O_4$ nanoparticles after 50 cycles at the current density of 0.1 C.

Conclusions

In this work, the results of synthesis of core-shell structured $NiFe_2O_4$/onion-like carbon nanocapsules and influence of onion-

60 like carbon shells on the electrochemical properties of $NiFe_2O_4$ nanoparticles are presented. Owing to the synergistic effect of $NiFe_2O_4$ nanoparticles and onion-like C shells as well as the special core/shell structure, the $NiFe_2O_4$/onion-like C nanocapsules exhibit superior electrochemical performance when

65 evaluated as anode materials for LIBs. At the current density of 0.1 C, the nanocapsules exhibits a discharge capacity of 914 mAh g^{-1} up to 500 charge-discharge cycles, which is much higher than that of $NiFe_2O_4$ nanoparticles. Varying the rate of charge/discharge current from 0.1 to 4 C does not show negative

70 effects on the recycling stability of the nanocapsules and a recoverable specific capacity as high as 914 mAh g^{-1} is obtained. EIS measurement shows the charge transfer resistance of $NiFe_2O_4$/onion-like C nanocapsules is smaller than that of the $NiFe_2O_4$ nanoparticles. Postmortem analysis of the

75 $NiFe_2O_4$/onion-like C nanocapsules after 500 cycles shows that the nanocapsules retain its morphology. The introduction of the onion-like C shell and the presence of the void spaces are found to increase the contact areas between the electrolyte and the nanocapsules for improved electrolyte diffusion, to enhance the

80 electronic conductivity and ionic mobility of the $NiFe_2O_4$ nanoparticle cores, and to accommodate the change in volume during the lithium-ion insertion/extraction process.

Acknowledgements

Notes and references

90 ^{a}College of Science, Northeast Dianli University, Jilin 132012, PR China. Fax/Tel:+86 432 64806631; E-mail: loveh_andan@163.com
† Electronic Supplementary Information (ESI) available: See DOI: 10.1039/b000000x/

1 C.Z. Yuan, J.Y. Li, L.R. Houm L.H. Zhang and X.G. Zhang, Part. Part.
95 Syst. Char. 2014, 31, 657-663.
2 Y.H. Xu, Q. Liu, Y.J. Zhu, Y.H. Liu, A. Langrock, M.R. Zachariah and C.S. Wang, Nano Lett. 2013, 13, 470-474.
3 N.N. Wang, H.Y. Xu, L. Chen, X. Gu, J. Yang and Y.T. Qian, J. Power Sources 2014, 247, 163-169.
100 4 Z.Q. Zhu, S.W. Wang, J. Du, Q. Jin, T.R. Zhang, F.Y. Cheng and J. Chen, Nano Lett. 2014, 14, 153-157.
5 J.F. Li, S.L. Xiong, Y.R. Liu, Z.C. Ju and Y.T. Qian, ACS Appl. Mater. Inter. 2013, 5, 981-988.
6 X.G. Liu, S.W. Or, C.G. Jin, Y.H. Lv, C. Feng and Y.P. Sun, Electrochim.
105 Acta 2013, 100, 140-146.
7 X.G. Liu, N.N. Bi, C. Feng, S.W. Or and Y.P. Sun, J. Alloys Compd. 2014, 587, 1-5.
8 X.G. Liu, Y.P. Sun, C. Feng, C.G. Jin and F. Xiao, J. Power Sources 2014, 245, 256-261.
110 9 X.G. Liu, S.W. Or, C.G. Jin, Y.H. Lv, C. Feng and Y.P. Sun, Carbon 2013, 60, 215-220.
10 X.G. Liu, G.P. Zhou, S.W. Or and Y.P. Sun, RSC Adv. 2014, 4, 51389-51394.
11 P.P. Lv, H.L. Zhao, Z.P. Zeng, J. Wang, T.H. Zhang and X.W. Li, J.
115 Power Sources 2014, 259, 92-97.
12 H.W. Liu and H.F. Liu, J. Electron. Mater. 2014, 48, 2553-2558.
13 M. Yehia, Sh. Labib and S.M. Ismail, Phys. B 2014, 446, 49-54.

14 H.W. Liu, H. Zhu and H.M. Yang, Mater. Res. Bull. 2013, 48, 1587-1592.

15 P. Lavela and J.L. Tirado, J. Power Sources 2007, 172, 379-387.

16 Y.N. Nuli and Q.Z. Qin, J. Power Sources 2005, 142, 292-297.

17 G. Huang, F.F. Zhang, X.C. Du, J.W. Wang, D.M. Yin and L.M. Wang, Chem. Eur. J. 2014, 20, 11214-11219.

18 Z. Wang, X. Zhang, Y. Li, Z.T. Liu and Z.P. Hao, J. Mater. Chem. A 2013, 1, 6393-6399.

19 D.L. Chao, X.H. Xia, J.L. Liu, Z.X. Fan, C.F. Ng and Z.X. Shen, Adv. Mater. 2014, 6, 5794-5800.

20 C.Y. Cui, X.G. Liu, N.D. Wu and Y.P. Sun, Mater. Lett. 2015, 143, 35-37.

21 X.G. Liu, B. Li, D.Y. Geng, W.B. Cui, F. Yang and Z.G. Xie, Carbon 2009, 47, 478-484.

22 X.G. Liu, D.Y. Geng, J. Du, S. Ma, B. Li and P.J. Shang, Scripta Mater. 2008, 59, 340-343.

23 X.G. Liu, C.Y. Cui, N.D. Wu, S.W. Or and N.N. Bi, Ceram. Int. 2015,41, 7511-7518.

24 E.Paparazzo, J. Electron Spectrosc. Relat. Phemon. 1987, 43, 97-112.

25 H. Konno and M. Nagayama, J. Electron Spectrosc. Relat. Phemon. 1980, 18, 341-343.

26 D.W. Oscarson, P.M. Huang, C. Defosse and A. Herbillion, Nature 1981, 291, 50-51.

27 D.G. Zetaruk and N.S. McIntyre, Anal. Chem. 1977, 49, 1521-1529.

28 K.K. Lian, D.W. Kirk and S.J. Thorpe, J. Electrochem. Soc. 1995, 142, 3704-3712.

29 A.N. Mansour, Surf. Sci. Spectra 1994, 3, 321.

30 C.E. Dube, B. Workie, S.P. Kounaves, A. Robbat, M.L. Jr Aksu and G. Davies, J. Electrochem. Soc. 1995, 142, 3357-3365.

31 H.X. Zhao, Z. Zheng, K.W. Wong, S.M. Wang, B.J. Huang and D.P. Li, Electrochem. Commun. 2007, 9, 2606-2610.

32 C.T. Cherian, J. Sundaramurthy, M.V. Reddy, P.S. Kumar, K. Mani, D. Pliszka, C.H. Sow, S. Ramakrishna and B.V. R. Chowdari, ACS Appl. Mater. Interfaces 2013, 5, 9957-9963.

33 Y.S. Fu, Y.H. Wan, H. Xia and X. Wang, J. Power Sources 2012, 213, 338-342.

34 L.Y. Wang, L.H. Zhuo, C. Zhang and F.Y. Zhao, J. Power Sources 2015, 275, 650-659.

35 L.M. Sun, X.H. Wang, R.A. Susantyoko and Q. Zhang, Carbon 2015, 82, 282-287.

36 G.Q. Zhang, L. Yu, H.B. Wu, H.E. Hoster and X.W. Lou, Adv. Mater. 2012, 24, 4609-4613.

37 L. Zhou, H.B. Wu, T. Zhu and X.W. Lou, J. Mater. Chem. 2012, 22, 827-829.

38 S. Laruelle, S. Grugeon, P. Poizot, M. Dolle, L. Dupont and J.M. Tarascon, J. Electrochem. Soc. 2002, 149, A627-A634.

39 G.M. Zhou, D.W. Wang, F. Li, L.L. Zhang and H.M. Cheng, Chem. Mater. 2010, 22, 5306-5313.

40 J.Z. Chen, L. Yang, S.H. Fang and S.I. Hirano, Electrochem. Commun. 2011, 13, 848-851.

41 N. Yan, L. Hu, Y. Li, Y. Wang, H. Zhong and X.Y. Hu, J. Phys. Chem. C 2012, 116, 7227-7235.

42 X.W. Lou, D. Deng, J.Y. Lee and L.A. Archer, J. Mater. Chem. 2008, 18, 4397-4401.

43 C.Wang, D.L. Wang, Q.M. Wang and L. Wang, Electrochim. Acta 2010, 55, 6420-6425.

44 F.M. Zhang, B.Y. Geng and Y.J. Guo, Chem. Eur. J. 2009, 15, 6169-6174.

45 L.F. Shen, X.G. Zhang, E. Uchaker, C.Z. Yuan and G.Z. Cao, Adv. Energy Mater. 2012, 2, 691-698.

46 Y. Yu, Y.C. Zhu, J.W. Liang, L. Fan and Y.T. Qiao, Electrochim. Acta 2013, 111, 809-813.

47 J.F. Li, S.L. Xiong, Y.R. Liu, Z.C. Ju and Y.T. Qian, ACS Appl. Mater. Inter. 2013,5, 981-988.

48 L.L. Li, Y.L. Cheah, Y. Ko, P.F. The, G. Wee and C.L. Wong, J. Mater. Chem. A 2013, 1, 10935-10941.

49 Y. Shi, Z.J. Zhang, D. Wexler, S.L. Chou, J. Gao and H.J. Li, J. Power Sources 2015, 275, 392-398.